Adaptive real-time identification of motor unit discharges from non-stationary high-density surface electromyographic signals

Chen Chen, Shihan Ma, Xinjun Sheng*, Dario Farina, and Xiangyang Zhu*

Abstract*—*Objective. **Estimation of the discharge pattern of motor units by electromyography (EMG) decomposition has been applied for neurophysiologic investigations, clinical diagnosis, and human-machine interfacing. However, most of the methods for EMG decomposition are currently applied offline. Here, we propose an approach for high-density surface EMG decomposition in real-time.** ***Methods.*** **A real-time decomposition scheme including two sessions, offline training and online decomposition, is proposed based on the convolutional kernel compensation algorithm. The estimation parameters, separation vectors and the thresholds for spike extraction, are first computed during offline training, and then they are directly applied to estimate motor unit spike trains (MUSTs) during the online decomposition. The estimation parameters are updated with the identification of new discharges to adapt to non-stationary conditions. The decomposition accuracy was validated on simulated EMG signals by convolving synthetic MUSTs with motor unit action potentials (MUAPs). Moreover, the accuracy of the online decomposition was assessed from experimental signals recorded from forearm muscles using a signal-based performance metrics (pulse-to-noise ratio, PNR).** ***Main results.*** **The proposed algorithm yielded a high decomposition accuracy and robustness to non-stationary conditions. The accuracy of MUSTs identified from simulated EMG signals was $> 80\%$ for most conditions. From experimental EMG signals, on average, 12 ± 2 MUSTs were identified from each electrode grid with PNR of 25.0 ± 1.8 dB, corresponding to an estimated decomposition accuracy $> 75\%$.** ***Conclusion and Significance.*** **These results indicate the feasibility of real-time identification of motor unit activities non-invasively during variable force contractions, extending the potential applications of high-density EMG as a neural interface.**

***Index Terms*—real-time decomposition, motor unit, surface EMG, high-density**

I. Introduction

The motor unit, comprising a motor neuron together with all the muscle fibers it innervates, is the smallest functional unit in the neuromuscular system [1]. The discharges by the motor neuron correspond to action potentials of the innervated muscle fibers (muscle unit) [2] and therefore they can be identified by processing and decomposing electromyography (EMG) signals. Decomposition of EMG has found applications in neurophysiology [3], clinical diagnosis [4], and human-machine interfacing (HMI) [5]–[7].

C. Chen, S. Ma, X. Sheng and X. Zhu are with the State Key Laboratory of Mechanical System and Vibration, Shanghai Jiao Tong University, 800 Dongchuan Road, Shanghai, China

D. Farina is with the Department of Bioengineering, Imperial College London, London, UK

*Corresponding author: Xiangyang Zhu (mexyzhu@sjtu.edu.cn), Xinjun Sheng (xjsheng@sjtu.edu.cn)

The ensemble of motor neurons discharges contains the neural drive transferred from the spinal cord to the innervated muscle and provides direct information on the functional tasks associated to muscle activation [3], [8], [9]. Moreover, information on motor unit behavior has also contributed to better understanding the pathophysiological mechanisms of tremor [4], stroke [10], as well as the neural determinants of training and aging [11], [12]. As to HMI, interfaces based on EMG decomposition has shown better performance than classic myocontrol systems [5], [6], [13]. Farina *et al* have applied EMG decomposition for prosthetic control on patients following targeted muscle reinnervation, showing superior performance compared with conventional EMG-based control methods. [5]. Moreover, precise identification of wrist and finger movements has been proven feasible following EMG decomposition [7], [13], [14].

Motor unit activities can be decoded with electrodes either placed inside the muscle or mounted on the skin surface. Needle/wire electrodes have been used for this purpose since the 1920s [15]. Automatic algorithms for processing intramuscular signals have been proposed in the 1970s [16], [17] and progressively improved over time [18]–[20]. However, because of the high selectivity, intramuscular EMG (iEMG) can only identify relatively small samples of motor units, with fibers located close to the recording electrodes. Alternatively, motor unit activities can be identified in a non-invasive way by identifying action potentials from interference surface EMG signals through blind source separation [20]–[23] or template matching with machine learning [24], [25]. The surface EMG recording modality allows to measure motor unit properties that are difficult to access with invasive recordings (e.g., muscle fiber conduction velocity or location of end plates) and may increase the number of identified motor units compared to iEMG signals [26].

The decomposition approaches for surface EMG signals have been extensively validated in several muscles and contraction conditions [27]–[31]. However, currently most decomposition methods work offline because of the computational cost of the decomposition [4], [5], [9]. It is of utmost importance to achieve a real-time decomposition system for actual implementations such as prosthetic control and clinical diagnosis. Although several decomposition methods have been generalized to online conditions by pre-training the separation matrix, they are all limited within isometric contractions [32], [33]. In such conditions, the EMG signals are regarded as stationary and the non-stationarities are not taken into con-

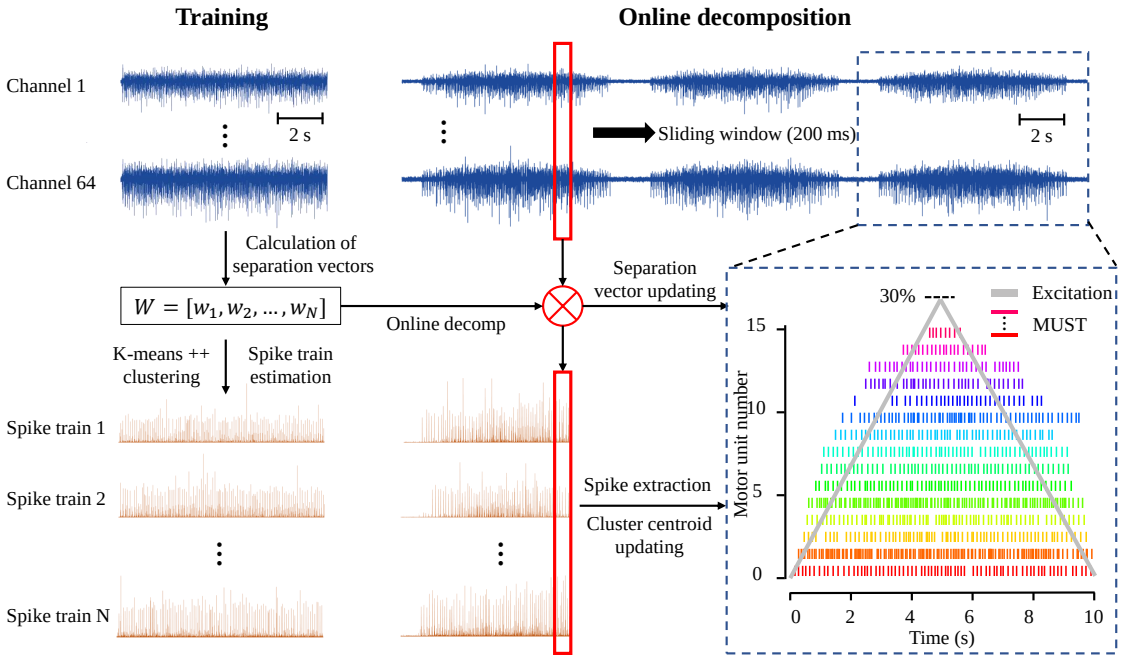

Fig. 1. The flow chart of the real-time decomposition algorithm.

sideration (e.g., excitation variation or muscle shortening). Recently, a decomposition method robust to changes of motor unit action potential (MUAP) has been proposed and can be used for the identification of motor unit firings during dynamic contractions. However, this method was still implemented offline.

Here, we propose a real-time decomposition approach for high-density surface EMG signals that can work online and on non-stationary signals. The performance of the proposed decomposition algorithm was tested with simulated and experimental EMG signals.

II. Algorithm

The decomposition algorithm includes two sessions, offline training and online decomposition (Fig.1). The estimation parameters, separation vectors for MUST estimation, and the thresholds for spike extraction, are first calculated in the offline session. In the online session, the spike trains are estimated in a sliding window by multiplying the separation vectors by the pre-processed EMG signals. Then the discharges are extracted depending on the trained thresholds. The estimation parameters are updated based on the newly identified discharges to adapt to non-stationary conditions.

A. Offline EMG decomposition

The surface EMG signals are first decomposed into MUSTs using the convolutional kernel compensation (CKC) algorithm in the offline session [23], [34]. The decomposition procedure is described in detail in [20], [34] and a brief explanation of its basic working principles is provided here.

The generation model of multi-channel surface EMG signals can be described as a convolutive mixture of a series of impulses, representing the discharge pattern of motor units [20]. The impulse responses of the filters in this mixture model are the action potentials of the motor units, which have a finite duration [23]. The mixing process can be written in matrix form as:

$$y(n) = H\bar{s} + \omega(n) \tag{1}$$

where $y(n) = [y_1(n), ..., y_M(n)]^T$ is the EMG signals for M channels, n is the sample point, $\omega(n)$ is the additive noise commonly modeled as a stationary and spatially while zero-mean Gaussian random process [23], $\bar{s}(n) = [s_1(n), s_1(n-1), ..., s_1(n-L+1), ..., s_N(n), s_N(n-1), ..., s_N(n-L+1)]^T$ is the extended vector from N sources, L is the length of action potentials, and H is the mixing matrix. The CKC method compensates the unknown mixing matrix H in equation (1) and estimates the spike train of the jth motor unit as:

$$\widehat{s}_j(n) = c_{s_j\bar{y}}^T C_{\bar{y}\bar{y}}^{-1} \bar{y}(n) \tag{2}$$

where $\bar{y}(n) = [y_1(n), y_1(n-1), ..., y_1(n-K+1), ..., y_i(n), y_i(n-1), ..., y_i(n-K+1), ..., y_M(n), y_M(n-1)..., y_M(n-K+1))]^T$ is the extended EMG signals by adding K delayed versions, $y_i(n)$ is the EMG signals of ith channel, K is the extending length and was set as 10 in this work. The EMG signals are extended to increase the ration between the number of observations (EMG channel) and the number of sources (MUST) [20], [23], [35]. $C_{\bar{y}\bar{y}} = E(\bar{y}(n)\bar{y}^T(n))$ is the correlation matrix of the extended EMG signals, $c_{s_j\bar{y}} = E(\bar{y}(n)s_j^T(n))$ is the cross-correlation vector, and $E(\cdot)$ denotes mathematical expectation. Suppose

$$w_j = C_{\bar{y}\bar{y}}^{-1} c_{s_j\bar{y}} \tag{3}$$

the estimation of spike train (equation (2)) can be written as:

$$\widehat{s}_j(n) = w_j^T \bar{y}(n) \tag{4}$$

where w_j is the separation vector for the jth motor unit. In this study, $c_{s_j\bar{y}}$ is estimated iteratively using the natural gradient descent algorithm [34].

The discharge pattern of each motor unit is extracted from the estimated spike trains using the Kmeans++ algorithm [20], [36]. The silhouette measurement (SIL) is used to quantify the clustering quality [20]. During offline decomposition, only MUSTs with SIL $>$ 0.8 are kept for the following online decomposition.

After the offline decomposition, the cross-correlation vectors ($c_{s_j\bar{y}}$), the correlation matrix of EMG signals ($C_{\bar{y}\bar{y}}$), and the cluster centroids are stored for later use in the online decomposition procedure.

B. Online EMG decomposition

During the offline decomposition, the iteration for MUST estimation and the clustering for spike extraction are time consuming and therefore cannot be implemented online. For real-time decomposition, the spike trains are estimated according to Eq. 2, where $c_{s_j\bar{y}}$ and $C_{\bar{y}\bar{y}}$ are obtained from the offline session. Then the motor unit discharges are extracted from $\widehat{s}_j(n)$ by comparing the Euclidian distance to the cluster centroids.

Application of the separation vectors obtained in the offline phase to the online decomposition would assure EMG decomposition in the online phase only if the signal properties remain similar between the offline and online phases, i.e. if the signal is stationary. Conversely, in general conditions, the initial separation vectors need continuous adaptation.

In order to adapt to non-stationary conditions, we propose a method for adapting the separation vector w_j each time a new discharge is identified. For this purpose, the components to calculate the separation vector ($c_{s_j\bar{y}}$ and $C_{\bar{y}\bar{y}}$) are updated as:

$$C_{\bar{y}\bar{y}} = C_{\bar{y}\bar{y}} + C_{\triangle\bar{y}\triangle\bar{y}} \tag{5}$$

$$c_{s_j\bar{y}} = c_{s_j\bar{y}} + \ell \cdot \frac{1}{card(\Psi_j)} \sum_{n_k \in \Psi_j} \triangle\bar{y}(n_k) \tag{6}$$

where $\Psi_j = \{n_1, n_2, ...\}$ is the group of the newly identified discharges. ℓ is the learning rate, which was set as 0.1 empirically in this study. $\triangle\bar{y}$ is the extended EMG signals in the sliding window.

The cluster centroids are also updated as:

$$T_{ij} = \frac{w_1 T_{ij} + w_2 T_{ij}^{'}}{w_1 + w_2}, i = 1, 2 \tag{7}$$

where T_{ij} is the previous centroid of discharges ($i = 1$) or noise ($i = 2$) for the jth MUST, $T_{ij}^{'}$ is the new centroid obtained in the sliding window, w_1 and w_2 are the weights added on the centroids. In this study, w_1 was set as 5, empirically, and w_2 was set as the number of the newly identified discharge or noise timings. Fig.2 illustrates an example result of the MUST estimation and spike extraction during a simulated non-isometric contraction.

The pseudocode of the proposed adaptive decomposition method is shown in Algorithm 1.

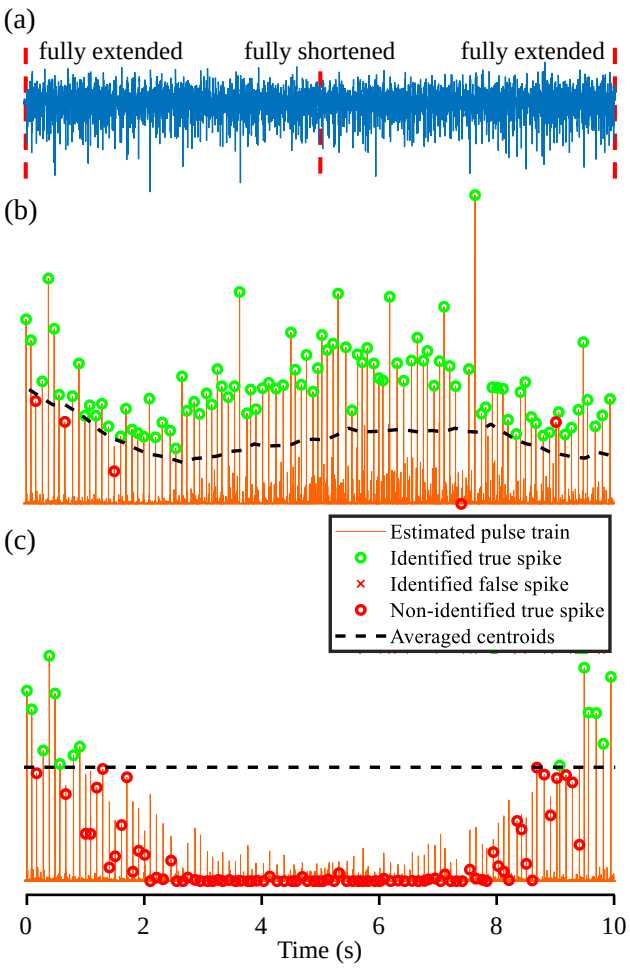

Fig. 2. Spike extraction under non-isometric contractions. (a) A 10-s-long EMG signal during a simulated dynamic contraction with changes in muscle length. (b) A spike train estimated from the simulated signals with the proposed update strategy. (c) The spike train same as (b) but estimated without the update strategy.

III. Methods

In this study, the proposed decomposition algorithm was first validated on synthetic EMG signals under multiple conditions. The synthetic EMG signals were obtained by convolving simulated MUSTs with MUAPs. Then the proposed algorithm was tested on experimental signals.

A. Simulated EMG signals

The MUAPs were simulated with a multi-layer cylindrical volume conductor model, compromising three layers (muscle, fat, and skin) [37]. The simulated muscle tissue comprised $>$ 4000 fibers with an average diameter of 56 μm. The fibers were grouped into 100 muscle units, with a number of fibers in the range 25-2500. The motor units had a normally distributed conduction velocity of 4.0$\pm$0.35 m/s, with the slowest velocity assigned to the smallest motor unit [38]. The simulated detection system was a grid of 11$\times$11 circular electrodes (radius 1 mm) with inter-electrode distance of 2.5 mm along both directions. For the results presented here, 64 channels (8$\times$8) in the grid center were used.

Algorithm 1 The proposed real-time decomposition method

1: Decode the MUSTs offline (given that N motor units were identified, $ST_1, ST_2, ..., ST_N$).
2: Load the estimation parameters, $c_{s_j\bar{y}}$, $C_{\bar{y}\bar{y}}$, T_{1j} (the jth centroid for the spikes), T_{2j} (the jth centroid for the base-line noise).
3: **while** Acquiring EMG signals **do**
4: Extract the EMG signals of 200 ms.
5: Filter the signals and extend the EMG signals ($\triangle\bar{y}$).
6: Calculate the correlation matrix of $\triangle\bar{y}$, $C_{\bar{y}\bar{y}} = E(\triangle\bar{y}(n) \triangle \bar{y}^T(n))$.
7: Update the correlation matrix, $C_{\bar{y}\bar{y}} = C_{\bar{y}\bar{y}} + C_{\triangle\bar{y}\triangle\bar{y}}$.
8: **for** $j = 1; j \leq N; j++$ **do**
9: Estimate the jth MUST, $\widehat{s}_j(n) = c_{s_j\bar{y}}^T C_{\bar{y}\bar{y}}^{-1} \triangle\bar{y}(n)$.
10: Classify $\widehat{s}_j(n)$ into spike or base-line noise depending on the Euclidian distance to T_{1j} and T_{2j}.
11: Initialize $\Psi_j = \emptyset$ and put the newly identified spikes into Ψ_j, $\Psi_j = \{n_1, n_2, ..., n_k\}$.
12: Update $c_{s_j\bar{y}}$ with $\ell = 0.1$, $c_{s_j\bar{y}} = c_{s_j\bar{y}} + \ell \cdot \frac{1}{card(\Psi_j)} \sum_{n_k \in \Psi_j} \triangle\bar{y}(n_k)$.
13: Update T_{1j} and T_{2j} with $w_1 = 5$ and $w_2 = k$, $T_{ij} = \frac{w_1 T_{ij} + w_2 T'_{ij}}{w_1 + w_2}, i = 1, 2$.
14: $ST_j = ST_j \cup \Psi_j$.
15: **end for**
16: **end while**

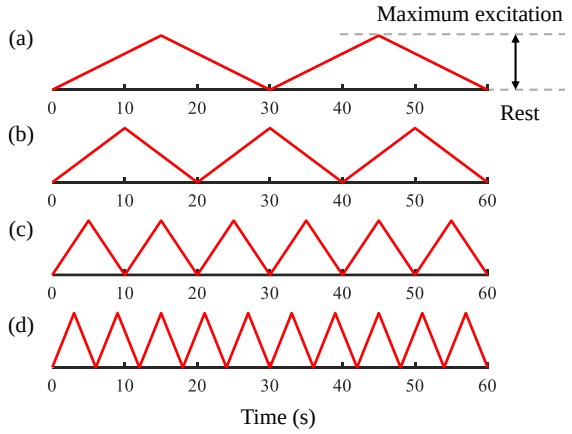

Fig. 3. Illustration of the profile of variations of excitation level.

The motor unit recruitment thresholds were distributed following an exponential function, in order of size [39], as previously modeled in [40]. Each motor unit discharged at 8 Hz when initially recruited, then the discharge rate increased at 0.3 Hz/% excitation until a maximum value of 35 Hz [40]. The inter-spike interval variability followed a Gaussian distribution with a coefficient of variation of 20%.

Three datasets of synthetic EMG signals were simulated (Sim1-Sim3). In dataset Sim1, three contraction conditions were simulated with different input excitation levels (10%, 30%, or 50%). In this dataset, the input excitation was constant and lasted for 70 s. The number of recruited motor units was 52 (10% excitation), 77 (30%), and 89 (50%).

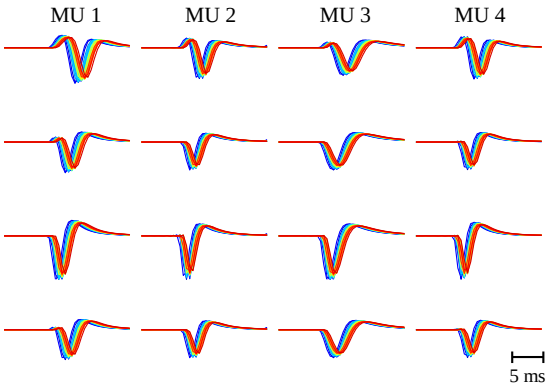

Fig. 4. Four simulated MUAPs with time-varying waveform shapes. Four channels from the center column of the grid are illustrated. Blue and red lines represent the MUAP shapes with muscle fully shortened and fully extended, respectively.

In dataset Sim2, the excitation was constant for 10 s and then varied over time for 60 s, as shown in Fig.3. The variations over time were in cycles of durations 30 s, 20 s, 10 s, and 6 s (Fig.3 (a)-(d)). There were 12 conditions in total (3 excitation levels $\times$ 4 excitation changing speeds) in dataset Sim2.

In dataset Sim3, the excitation level was maintained constant but the MUAP waveforms changed over time. The muscle shortening affects the MUAP shapes acting as a low-pass filter that suppresses high frequencies [41], [42]. The MUAP waveforms were varied by stretching the MUAP duration and compressing the MUAP amplitude:

$$g'(x) = \frac{1}{\gamma} g(\frac{x}{\gamma}) \tag{8}$$

where $g(x)$ is the raw MUAP waveforms, $g'(x)$ is the changed waveforms, and γ is the coefficient of stretching and compressing (Fig.4). The coefficient γ was set to 1.2 under fully extended conditions. The profiles for variation of γ were the same as those for the variations of excitation level in Sim2, with 12 conditions in total (3 excitation levels $\times$ 4 MUAP changing speeds).

The synthetic EMG signals were generated as the convolution of MUSTs and MUAPs. colored zero-mean Gaussian noise with signal-to-noise ratio (SNR) 10-30 dB (5 dB increments) was added to the simulated signals. The simulated signals were sampled at 2048 Hz, and bandpass filtered between 20 and 500 Hz. We conducted 5 simulation runs for each condition in three datasets (27 conditions in total). In each simulation run, 100 motor units were randomly selected from a motor unit pool with over 400 motor units.

In each simulation run, the first 10-s signals were used for offline training, while the remaining 60-s signals were used to test the performance of the online decomposition. To investigate the effect of the update strategy for the estimation parameters, the simulated EMG signals were also decomposed without the update strategy, where the step 6, 7, 12, and 13 in Algorithm 1 were not performed during online decomposition.

Sensitivity and precision were used to evaluate the decomposition accuracy for each motor unit [41]:

$$\text{Sensitivity} = \frac{\text{TP}}{\text{TP} + \text{FN}} \tag{9}$$

$$\text{Precision} = \frac{\text{TP}}{\text{TP} + \text{FP}} \tag{10}$$

where TP (true positive) denotes the number of correctly identified discharges, FN (false negative) denotes the number of non-identified discharges, and FP (false positive) stands for the number of incorrectly identified discharges. In the decomposition of simulated EMG signals, only MUSTs with sensitivity $> 50\%$ were kept for the following analysis, which were regarded to be correctly identified.

A signal-based metrics, the pulse-to-noise ratio (PNR), was applied to evaluate the decomposition accuracy [28]. The PNR of the jth MUST was calculated as:

$$\text{PNR}_j = 10 \cdot \log\left(\frac{E(\widehat{s}_j(n)|_{\widehat{s}_j(n)\geq r})}{E(\widehat{s}_j(n)|_{\widehat{s}_j(n)<r})}\right) \tag{11}$$

where $E(x|_{\widehat{s}_j(n)\geq r})$ and $E(x|_{\widehat{s}_j(n)<r})$ denote the mean across all time moments in which the jth motor unit is estimated to have or not have discharged, respectively [28]. To investigate the correlation between two accuracy measurements and the PNR, a regression line $y = 100 - \frac{a_1}{(x-a_2)^4}$ was fitted with the nonlinear least-squares fitting method between the sensitivity/precision (y) and PNR (x), where a_1 and a_2 were the parameters to be trained.

All the simulations, decompositions, and analysis were implemented in MATLAB 2018b (Matlab Inc. USA).

B. Experimental EMG signals

Five able-bodied subjects (4 males, 1 female, aged 26±3 years) participated in the experiment. They had no neurological disorders, and signed an informed consent before participating to the experiments. The experiments were in compliance with the Declaration of Helsinki.

In the experiments, the subjects were instructed to finish three sessions of grasping tasks (Exp1-Exp3), corresponding to three simulated datasets.

- In the session of Exp1, subjects were instructed to perform isometric grasping with constant force at 10%, 30%, and 50% of the maximum voluntary contraction (MVC) force.
- In Exp2, subjects were instructed to follow a force trace as the one described in Sim2. Only ramps of 6 s at three levels were kept to simplify the experiment.
- In Exp3, subjects were instructed to perform non-isometric dynamic grasping, and the grasp cycle was set as 6 s. The subjects were instructed to try to keep the contraction level during dynamic grasping, but not strictly.

There were 9 conditions in total in the three experimental sessions and each condition included two identical trials. Each trial lasted for 40 s. The first 10-s signals were used for offline training, and the remaining 30-s signals were used for online decomposition, as in the simulations.

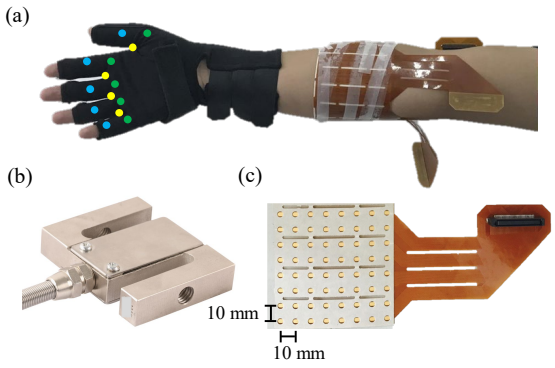

Fig. 5. Experimental setup. (a) The EMG recording area and the data glove used to measure dynamic grasping. Fourteen channels of finger angles, including 5 metacarpophalangeal joints (green circles), 5 proximal interphalangeal joints (blue circles), and 4 abduction angles (yellow circles), were recorded with the data glove. (b) The force transducer used to measure isometric grasping force. (c) The high-density electrode grid.

In Exp1 and Exp2, the grasping force was measured with a customized transducer (Fig.5(b)) and sampled at 2048 Hz. In Exp3, 14 channels of finger angles were recorded with a data glove (5 DT Data Glove 14 Ultra, 5DT Inc. USA) and sampled at 100 Hz (Fig.5(a)). The angles were averaged across the 14 channels to depict the dynamic grasp kinematics. During the experiments, the grasp force or angles were displayed on the screen to provide a visual feedback to the subjects.

High-density surface EMG signals were acquired with three electrode grids of 64 channels each (ELSCH064NM3, 8×8 channels, OT Bioelettronica, Italy). The grids were mounted around the proximal third of the forearm of the dominant arm. The electrode diameter was 3 mm with inter-electrode distance of 10 mm in both directions. The electrode grids were connected to a multichannel amplifier (EMG-USB2+, OT Bioelettronica, Italy), with a gain of 500 and sampling frequency of 2048 Hz. The experimental EMG signals were bandpass filtered between 20 and 500 Hz. In addition, a comb filter was applied to reject the 50-Hz power-line interference and its harmonics. The decomposition was applied to each grid separately.

IV. Results

The real-time decomposition was implemented with a sliding window of 200 ms. The calculation complexity of the MUST estimation and the updating process in the sliding window had computational cost $\leq$ 50 ms, resulting a delay $\leq$ 250 ms during online decomposition. The offline training took about 100 s for 10-s signals.

The decomposition results for simulated signals using the proposed real-time scheme are illustrated in Fig.6 - Fig.8. For simulated EMG signals with constant excitation and without changes in MUAP waveforms (dataset Sim1), on average, 35±3 (32±1, 30±3) MUSTs were identified correctly with sensitivity and precision $> 95\%$ at the excitation level of 10% (30%, 50%), when no additional noise was added. The number of correctly identified MUSTs decreased to 11±1 (8±0, 7±1) when noise was added at 10 dB SNR. Nevertheless, the

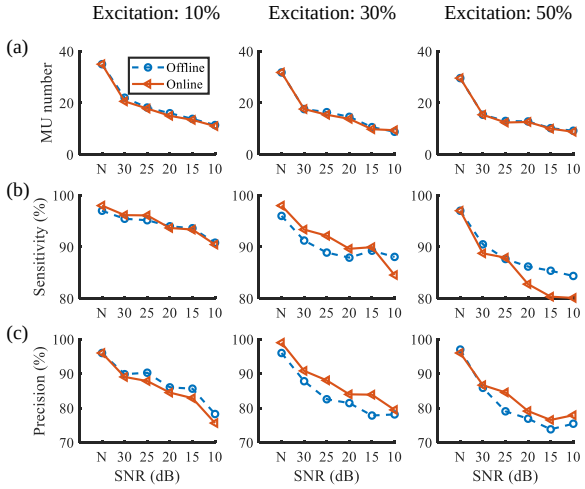

Fig. 6. Decomposition results for the dataset Sim1. (a) The average number of correctly identified MUSTs under different conditions. The MUSTs with sensitivity $< 50\%$ were discarded after decomposition. (b) and (c) illustrate the average sensitivity and precision of the identified MUSTs. N in the horizontal axis denotes conditions for which no noise was added to the simulated signals.

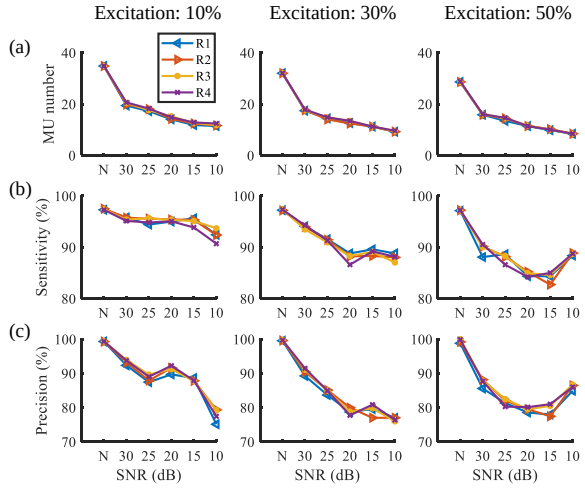

Fig. 7. Decomposition results for the dataset Sim2. (a)-(c) illustrate the average number of correctly identified MUSTs, sensitivity, and precision under different conditions, as in Fig.6. N in the horizontal axis denotes the conditions for which no noise was added. R1-R4 depicts four different excitation ramps (cycles from 30 s to 6 s).

average sensitivity and precision were both over 80% for these identified MUSTs from dataset Sim1.

For simulated EMG signals with varying excitation, the number of correctly identified MUSTs was always > 7, with sensitivity in decomposition $> 80\%$ and precision $> 70\%$. For simulated EMG signals with varying MUAP shapes, the average sensitivity was $> 80\%$ in all cases and the precision was $> 70\%$ in all cases with the exception of a few conditions. The relation between PNR and the two accuracy measurements is illustrated in Fig.9.

The comparison between decomposition results with or without update strategy are shown in Fig.10. There was no significant difference between the two methods for the decomposition results in dataset Sim1 and Sim2, whereas the update

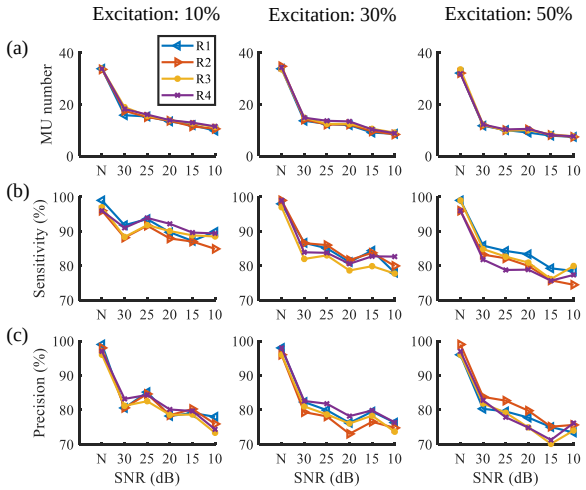

Fig. 8. Decomposition results for the dataset Sim3. (a)-(c) illustrate the average number of correctly identified MUSTs, sensitivity, and precision under different conditions, as in Fig.6. N in the horizontal axis denotes the conditions for which no noise was added. R1-R4 depicts four different MUAP varying ramps (cycles from 30 s to 6 s).

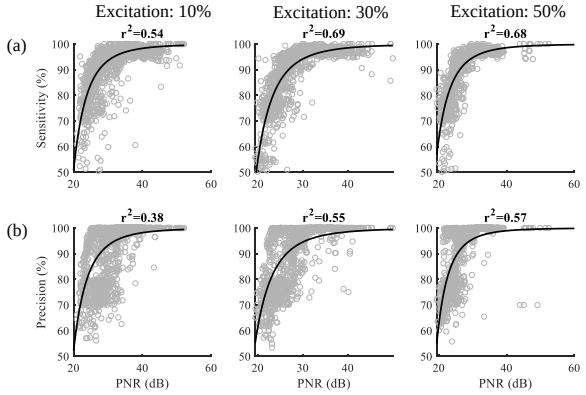

Fig. 9. Relation between the PNR and two decomposition accuracy measurements. The results are accumulated over all simulations with the specific excitation levels.

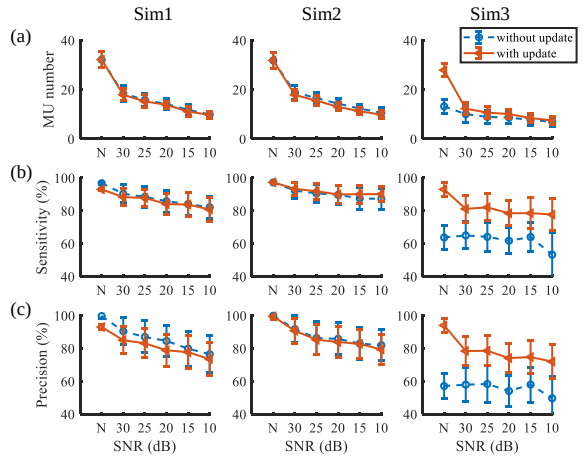

Fig. 10. The decomposition results with or without update strategy. (a)-(c) illustrate the average number of correctly identified MUSTs, sensitivity, and precision for three simulation datasets. The results were averaged across all simulation runs of three excitations.

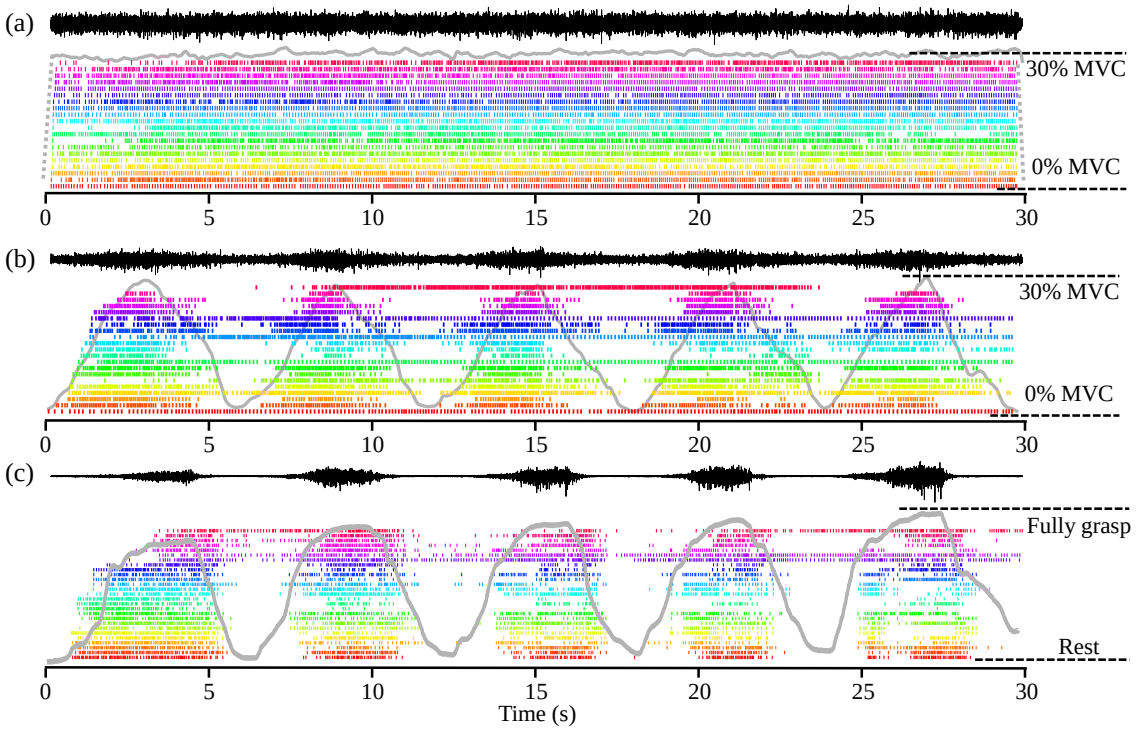

Fig. 11. Representative decomposition results of experimental EMG signals recorded with grid 2 from subject 4. (a)-(c) illustrate the decomposition results corresponding to session Exp1-Exp3 in the experiments. Black lines depict the EMG signals. Each vertical bar depicts one motor unit discharge, with different MUSTs depicted in different colors. The kinematics (force-(a)(b) or angle-(c)) are depicted in grey lines.

TABLE I
SUMMARY OF DECOMPOSITION RESULTS FOR EXPERIMENTAL EMG SIGNALS

Session	Excitation	Number of motor units				PNR of motor units (dB)		SNR of EMG (dB)	
		Grid 1	Grid 2	Grid 3	All	Offline	Online	Offline	Online
1	10%	14±6	9±4	15±5	39±11	29.0±1.9	22.8±5.2	13.3±1.7	11.8±1.6
	30%	13±5	7±5	12±3	34±11	28.9±1.7	23.6±5.7	20.2±2.7	19.8±3.1
	50%	15±10	10±4	11±4	38±16	28.8±1.5	23.5±5.1	25.2±2.1	24.8±3.1
2	10%	14±4	8±4	10±4	33±6	28.9±1.6	23.7±5.9	14.1±1.5	13.5±2.2
	30%	13±3	7±4	10±6	29±9	28.8±1.5	23.7±6.0	20.8±3.6	19.1±2.8
	50%	13±5	9±3	13±6	33±8	29.3±1.8	26.2±7.5	22.8±4.6	20.9±4.7
3	10%	13±7	12±7	12±5	37±13	29.2±2.0	26.1±5.7	14.9±2.2	17.4±3.9
	30%	11±5	9±2	9±4	29±6	28.9±1.4	26.3±5.8	18.6±6.1	22.2±8.2
	50%	17±13	12±5	11±4	42±20	29.1±1.6	28.7±6.4	24.5±3.6	26.8±4.2

strategy improved the decomposition accuracy significantly in Sim3, with the increase of sensitivity or precision of about 20%.

Fig.11 illustrates an example of decomposition results for experimental EMG signals at 30% contraction level. In Fig.11(c), the decrease of the grey line means that the subject stopped grasping and was opening the hand, resulting that most motor units stopped firing since they were identified during grasping tasks. The detailed decomposition results can be seen in Tab. I. The average PNR of MUSTs identified from online decomposition was greater than 24 dB, corresponding to sensitivity $\geq$ 80% and precision $\geq$ 75%.

V. DISCUSSION

An adaptive real-time decomposition method for the identification of motor units was proposed based on high-density surface EMG signals and validated with simulated and experimental signals. The results demonstrated good decomposition accuracy and robustness under non-stationary conditions. The processing delay including signal recording and computation was $\leq$ 250 ms, demonstrating the feasibility of applying the proposed method for real-time neural interfacing.

The EMG mixing process is typically modelled as a multiple-input-multiple-output system by linearly convolving the MUSTs and the MUAPs using Equ. 1. In isometric contractions, the MUAPs recorded by the surface electrodes are relatively stationary, and therefore have been assumed constant in several offline decomposition algorithms [20], [23]. In isometric contractions, the EMG non-stationarity mainly results from motor unit recruitment/derecruitment and discharge rate modulation. These two factors only affect the source signals in Equ. 1 rather than the mixture process. Therefore,

the update strategy had weak effect on the decomposition accuracy in Sim1 and Sim2, as Fig.10 shows. Nevertheless, the high accuracy of the decomposition results in Sim1 and Sim2 demonstrated that the proposed method is robust to motor unit recruitment/derecruitment or firing rate variation, and could decode MUSTs in real time during isometric contractions.

As to the dynamic non-isometric contractions, the changes in muscle length influence the relative position between the muscle fibers and the surface electrodes, and results in changes in MUAP waveforms and the following mixture process. In the CKC-based decomposition algorithm, the separation vectors are calculated based on the mixture process. The mixture matrix H in Equ. 1 is constant in isometric contractions, but varies over time in non-isometric conditions, which requires the corresponding update of separation vectors. Therefore, we proposed an update strategy for the separation vectors ($C_{\bar{y}\bar{y}}^{-1} c_{s_j \bar{y}}$) to trace the changing in mixing matrix. In dataset Sim3, the decomposition accuracy with the update strategy was significantly greater than that without updating, demonstrating the robustness of the proposed method to changes in MUAP shape during non-isometric contractions.

The non-stationary factors (varying excitations or MUAPs) had a small influence on the decomposition accuracy with the proposed update strategy, as the average sensitivity or precision of the correctly identified MUSTs in dataset Sim2 or Sim3 were only slightly lower than that in Sim1 in most conditions. It is noteworthy that neither the number of correctly identified MUSTs nor their accuracy measurements changed considerably when the rate of change in excitation or MUAP waveform shapes increased, regardless of the excitation or noise level, showing the robustness of the proposed decomposition scheme to the speed of non-stationarities. Compared with the non-stationary factors, the noise level had more significant effects on the decomposition accuracy. The number of correctly identified MUSTs and the corresponding accuracy measurements decreased substantially with increasing noise level. For this reason, increasing the SNR by improving the signal pre-processing can be an efficient way to improve decomposition accuracy. In this work, only the intrinsic non-stationarities (excitation or MUAP varying) were taken into consideration. As to the clinical application, several extrinsic factors such as sweating and electrode misplacement, may affect the actual implementation performance and should also be taken into consideration. In the future, the proposed method will be further validated in real-life applications such as clinical diagnosis and HMI systems.

The number of correctly identified MUSTs slightly declined with the increase of excitation level, which is likely caused by the increase in complexity of the mixing process. The number of accurately identified MUSTs in real-time from simulated stationary signals was always ≥ 10 and comparable to the results of offline decomposition. This number was also related to the number of decomposition runs in the offline training. In this study, the number of decomposition runs was set to 100. The number of accurately identified MUSTs may increase with the number of decomposition runs, at the cost of computational time in the offline training. The time cost of offline training will slightly affect the decomposition accuracy of online step, since the EMG signals during the offline decomposition were assumed to be stationary and could not be adapted. However, the real-time decomposition results still showed over 70% accuracy for non-stationary conditions, demonstrating the efficiency of the proposed approach.

The offline decomposition methods have been generalized into online conditions in several reports [32], [33], while most of which are limited in isometric contractions. The EMG signals are usually assumed to be stationary and the non-stationarities are not taken into consideration. Methods for identification of motor unit discharges during dynamic muscle contractions have been investigated, but limited in offline conditions [41]. In this work, the proposed decomposition approach could not only realize the real-time identification of motor unit discharges, but also adapt to the non-stationary conditions. It should be noted that the online decomposition accuracy of the proposed algorithm was slightly lower than the offline decomposition in [41]. For the purpose of real-time decomposition, the MUSTs were estimated by directly multiplying the trained separation vectors and the pre-processed EMG signals. However, in the offline decomposition, the separation vectors are calculated iteratively to optimize the estimation of MUSTs, increasing the discrimination capacity between discharges and noise. The difference in separation procedure explains the slight decrease in decomposition accuracy without iteration.

The signal-based measurement, PNR, has been previously demonstrated to be highly correlated with the decomposition accuracy [28], [41]. Similarly, the PNR increased monotonically with the real-time decomposition accuracy in this work. The simulation results demonstrated that the PNR was a reliable measurement to evaluate the online decomposition performance. Moreover, compared with sensitivity or precision, the calculation of the PNR needs no prior information of the motor unit activities. Therefore, the PNR was used to evaluate the decomposition accuracy for experimental EMG signals. The average PNR of MUSTs identified in the online decomposition was slightly lower than that in offline decomposition, which was caused by the difference of the separation procedure, as discussed above.

The feasibility of applying decoding techniques to HMI has been demonstrated in previous work [5], [7], [14]. However, these previous studies were all performed offline. In this study, a real-time decomposition algorithm was tested on experimental EMG signals recorded from forearm muscles during grasping tasks. The identified motor unit activities were highly correlated with the grasping kinematics (e.g. Fig.11), indicating the potential for the real-time HMI based on neural signals.

VI. Conclusion

We have proposed a real-time decomposition method for the identification of motor unit discharges based on high-density surface EMG signals. The proposed algorithm demonstrated high decomposition accuracy and robustness to variation of excitations and MUAP waveforms. These results support the wide application of EMG decoding techniques for neural interfacing.

ACKNOWLEDGMENT

The authors appreciate the valuable assistance about EMG simulation from Dr. Ning Jiang (University of Waterloo, Canada). This work is supported by in part the National Natural Science Foundation of China (No.91748119, No.51620105002), by the Science and Technology Commission of Shanghai Municipality (No.18JC1410400), and by the European Research Council Synergy Project Natural Bionics (No.810346).

REFERENCES

[1] M. Weinberger and J. O. Dostrovsky, *Motor Unit*. Oxford: Academic Press, 2010, pp. 204–206.
[2] C. Heckman and R. M. Enoka, *Motor Unit*. American Cancer Society, 2012, pp. 2629–2682.
[3] D. Farina, F. Negro, and J. L. Dideriksen, "The effective neural drive to muscles is the common synaptic input to motor neurons," *J Physiol*, vol. 592, no. Pt 16, pp. 3427–41, 2014.
[4] A. Holobar, *et al.*, "Non-invasive characterization of motor unit behaviour in pathological tremor," *Journal of Neural Engineering*, vol. 9, no. 5, p. 056011, 2012.
[5] D. Farina, *et al.*, "Man/machine interface based on the discharge timings of spinal motor neurons after targeted muscle reinnervation," *Nature Biomedical Engineering*, vol. 1, no. 2, p. 0025, 2017.
[6] C. Chen, *et al.*, "Hand gesture recognition based on motor unit spike trains decoded from high-density electromyography," *Biomedical Signal Processing and Control*, vol. 55, p. 101637, 2020.
[7] ——, "Prediction of finger kinematics from discharge timings of motor units: implications for intuitive control of myoelectric prostheses," *Journal of Neural Engineering*, vol. 16, no. 2, p. 026005, 2019.
[8] D. Farina, F. Negro, and N. Jiang, "Identification of common synaptic inputs to motor neurons from the rectified electromyogram," *J Physiol*, vol. 591, no. Pt 10, pp. 2403–18, 2013.
[9] C. Dai, *et al.*, "Origins of common neural inputs to different compartments of the extensor digitorum communis muscle," *Sci Rep*, vol. 7, no. 1, p. 13960, 2017.
[10] X. Li, *et al.*, "Examination of poststroke alteration in motor unit firing behavior using high-density surface emg decomposition," *IEEE Transactions on Biomedical Engineering*, vol. 62, no. 5, pp. 1242–1252, 2015.
[11] K. Watanabe, *et al.*, "Age-related changes in motor unit firing pattern of vastus lateralis muscle during low-moderate contraction," *AGE*, vol. 38, no. 3, p. 48, 2016.
[12] M. Piasecki, *et al.*, "Long-term endurance and power training may facilitate motor unit size expansion to compensate for declining motor unit numbers in older age," *Frontiers in Physiology*, vol. 10, no. 449, 2019.
[13] T. Kapelner, *et al.*, "Predicting wrist kinematics from motor unit discharge timings for the control of active prostheses," *Journal of NeuroEngineering and Rehabilitation*, vol. 16, no. 1, p. 47, 2019.
[14] ——, "Decoding motor unit activity from forearm muscles: Perspectives for myoelectric control," *IEEE Transactions on Neural Systems and Rehabilitation Engineering*, vol. 26, no. 1, pp. 244–251, 2018.
[15] E. D. Adrian and D. W. Bronk, "The discharge of impulses in motor nerve fibres," *The Journal of Physiology*, vol. 67, no. 2, pp. 9–151, 1929.
[16] D. Farina, *et al.*, "Multichannel thin-film electrode for intramuscular electromyographic recordings," *J Appl Physiol (1985)*, vol. 104, no. 3, pp. 821–7, 2008.
[17] R. Merletti and D. Farina, "Analysis of intramuscular electromyogram signals," *Philosophical Transactions: Mathematical, Physical and Engineering Sciences*, vol. 367, no. 1887, pp. 357–368, 2009.
[18] T. Yu, *et al.*, "Recursive decomposition of electromyographic signals with a varying number of active sources: Bayesian modelling and filtering," *IEEE Transactions on Biomedical Engineering*, pp. 1–1, 2019.
[19] J. Roussel, *et al.*, "Decomposition of multi-channel intramuscular emg signals by cyclostationary-based blind source separation," *IEEE Transactions on Neural Systems and Rehabilitation Engineering*, vol. 25, no. 11, pp. 2035–2045, 2017.
[20] F. Negro, *et al.*, "Multi-channel intramuscular and surface EMG decomposition by convolutive blind source separation," *Journal of Neural Engineering*, vol. 13, no. 2, p. 026027, 2016.
[21] M. Chen, *et al.*, "Automatic implementation of progressive fastica peel-off for high density surface EMG decomposition," *IEEE Trans Neural Syst Rehabil Eng*, vol. 26, no. 1, pp. 144–152, 2018.
[22] A. Holobar and D. Farina, "Blind source identification from the multichannel surface electromyogram," *Physiological Measurement*, vol. 35, no. 7, p. R143, 2014.
[23] A. Holobar and D. Zazula, "Multichannel blind source separation using convolution kernel compensation," *IEEE Transactions on Signal Processing*, vol. 55, no. 9, pp. 4487–4496, Sept 2007.
[24] C. J. De Luca, *et al.*, "Decomposition of surface EMG signals from cyclic dynamic contractions," *Journal of Neurophysiology*, vol. 113, no. 6, pp. 1941–1951, 2014.
[25] S. H. Nawab, S.-S. Chang, and C. J. De Luca, "High-yield decomposition of surface EMG signals," *Clinical Neurophysiology*, vol. 121, no. 10, pp. 1602–1615, 2010.
[26] R. Merletti, A. Holobar, and D. Farina, "Analysis of motor units with high-density surface electromyography," *J Electromyogr Kinesiol*, vol. 18, no. 6, pp. 879–90, 2008.
[27] A. Holobar, *et al.*, "Experimental analysis of accuracy in the identification of motor unit spike trains from high-density surface EMG," *IEEE Transactions on Neural Systems and Rehabilitation Engineering*, vol. 18, no. 3, pp. 221–229, 2010.
[28] A. Holobar, M. Minetto, and D. Farina, "Accurate identification of motor unit discharge patterns from high-density surface EMG and validation with a novel signal-based performance metric," *Journal of Neural Engineering*, vol. 11, no. 1, p. 016008, 2014.
[29] X. Hu, W. Z. Rymer, and N. L. Suresh, "Assessment of validity of a high-yield surface electromyogram decomposition," *Journal of Neuroengineering and Rehabilitation*, vol. 10, no. 1, p. 99, 2013.
[30] ——, "Accuracy assessment of a surface electromyogram decomposition system in human first dorsal interosseus muscle," *Journal of Neural Engineering*, vol. 11, no. 2, p. 026007, 2014.
[31] M. Chen, *et al.*, "Two-source validation of progressive fastica peel-off for automatic surface EMG decomposition in human first dorsal interosseous muscle," *International Journal of Neural Systems*, vol. 28, no. 09, p. 1850019, 2018.
[32] V. Glaser, A. Holobar, and D. Zazula, "Real-time motor unit identification from high-density surface EMG," *IEEE Transactions on Neural Systems and Rehabilitation Engineering*, vol. 21, no. 6, pp. 949–958, Nov 2013.
[33] Y. Zheng and X. Hu, "Real-time isometric finger extension force estimation based on motor unit discharge information," *Journal of Neural Engineering*, 2019.
[34] A. Holobar and D. Zazula, "Gradient convolution kernel compensation applied to surface electromyograms," in *International Conference on Independent Component Analysis and Signal Separation*. Springer, 2007, pp. 617–624.
[35] M. Chen, X. Zhang, and P. Zhou, "A novel validation approach for high-density surface EMG decomposition in motor neuron disease," *IEEE Transactions on Neural Systems and Rehabilitation Engineering*, vol. 26, no. 6, pp. 1161–1168, 2018.
[36] Y. Ning, *et al.*, "Surface EMG decomposition based on k-means clustering and convolution kernel compensation," *IEEE Journal of Biomedical and Health Informatics*, vol. 19, no. 2, pp. 471–477, 2015.
[37] D. Farina, *et al.*, "A surface emg generation model with multilayer cylindrical description of the volume conductor," *IEEE Trans Biomed Eng*, vol. 51, no. 3, pp. 415–26, 2004.
[38] ——, "Detecting the unique representation of motor-unit action potentials in the surface electromyogram," *J Neurophysiol*, vol. 100, no. 3, pp. 1223–33, 2008.
[39] E. HENNEMAN, "Relation between size of neurons and their susceptibility to discharge," *Science*, vol. 126, no. 3287, pp. 1345–1347, 1957.
[40] A. J. Fuglevand, D. A. Winter, and A. E. Patla, "Models of recruitment and rate coding organization in motor-unit pools," *Journal of Neurophysiology*, vol. 70, no. 6, pp. 2470–2488, 1993.
[41] V. Glaser and A. Holobar, "Motor unit identification from high-density surface electromyograms in repeated dynamic muscle contractions," *IEEE Transactions on Neural Systems and Rehabilitation Engineering*, vol. 27, no. 1, pp. 66–75, 2019.
[42] R. Merletti and D. Farina, *Surface electromyography: physiology, engineering, and applications*. John Wiley & Sons, 2016.